Characterization of the Tensile Behavior of EPS Foam as a Function of Density and Strain Rate

D. Zouzias*, G. D. Bruyne, R. Miralbes, J. Ivens

Prof J. Ivens
Dep. of Materials Engineering
KU Leuven
De Nayerlaan 5, B-2860, Sint-Katelijne Waver Belgium

G. D. Bruyne
LazerSport
Lamorierestraat 33, 2018, Antwerp, Belgium
+3232160900

R. Miralbes
Departamento de Ingeniería de Diseño y Fabricación
University of Zaragoza, Zaragoza
C/María de Luna, 3. 50018 Zaragoza

*Corresponding Author
KU Leuven
Dep. of Materials Engineering,
De Nayerlaan 5, B-2860, Sint-Katelijne Waver Belgium
email: dimitrios.zouzias@kuleuven.be

Keywords: polystyrene, tensile, properties, strain rate, density

ABSTRACT

Expanded polystyrene (EPS) foam is a material, frequently used in a range of applications for its good energy absorption, thermal insulation, durability, acoustic absorption and low thermal conductivity. In this wide range of applications, the material undergoes a variety of loads that can extend from static to dynamic. When it comes to crush applications, these loading profiles create the need of well-defined compression and tensile properties for a range of densities and strain rates. In this study, static and dynamic tension tests are conducted on EPS foam dog-bone samples for material characterization. The target of the study is to obtain stress-strain curves for a range of densities spreading from 60 g/l to 120 g/l. For the low strain rates, tensile

testing machines are used while for the high strain rates, a modified drop tower set-up was used. The influence of the strain rate on the stress-strain behavior, the dynamic strength, Young's modulus and energy absorption capacities for different foam densities is measured. Furthermore, the experimental results for each density are compared with the predictions of Avalle's model for crushable foams to evaluate the validity of the model. The quality of fit obtained between experimental and theoretical is between 70% - 97% depending on the strain rate.

1. INTRODUCTION

Due to its high energy absorbing efficiency [1][2] foam materials are widely used for protection in crush applications. Even though such applications vary in environmental and loading conditions, when it comes to helmets liners, static and dynamic loads are expected during the life cycle of the product. Such loads can be experienced during storage conditions, accidental or impact loads. Despite the stochastic profile of such loads, each foam material is expected to retain its functionality in all environmental conditions to which it will be exposed. For that reason a range of standards is created to describe the expected performance of these materials when integrated into protective headgear. Out of all the available choices, Expanded Polystyrene (EPS) is the most preferable of all, for its thermal and moisture resistance, light weight, durability availability and cost. This creates a big range of safety applications where it is crucial to be able to accurately predict the behavior of EPS.

As reported by A. Lorna [3] foams, another term for a cellular solid, are made up of an interconnected network of solid shells which form the edges and faces of cells. These cells can be either closed- or open celled and are spread as a three-dimensional polyhedral in space. EPS is a rigid and tough, recyclable, closed-cell cellular material. It can undergo a large compressive deformation and absorb energy even at high strain rates. Under compressive loads, energy is dissipated through cell bending, buckling or fracture. Its large energy absorbing properties are the result of the plateau that is observed in the characteristic compressive stress strain curve of the material. [7][8][9]. When closed-cell EPS foam is subjected to compressive loading, the entrapped air within the cells is compressed and additional viscous force is generated. Those forces increase with the loading rate, which results to the increase of strain rate sensitivity [8]

Constitutive material models

Foams are multi-phase materials. The gas-phase that is present in foams adds an additional degree of freedom which makes modelling of foams more difficult. There are several models available for various types of foams (rigid, flexible) and loading, but the models are usually limited, which makes the formulation of all the relevant behaviors of the foam difficult. The Maxwell model is a viscoelastic model. It consists of a spring and a damper in series, where elastic response is represented by the spring and the time-dependent response by the damper. The constitutive equation for this model is described by (Equation 1)

$$\sigma = E^{*}\dot{\varepsilon}\tau\left[1-\exp\left(-\frac{\varepsilon}{\tau\dot{\varepsilon}}\right)\right] \quad \text{(Equation 1)}$$

Where E is the Young modulus, τ is the relaxation time constant, ε is the strain and ἑ is the strain rate. The Maxwell material model is suited for a wide range of thermoplastic foams but more realistic material responses can be achieved by using non-linear models. At high strain rates the curves of the Maxwell model are expected to give a more linear estimation which might not be realistic. The springs in the Maxwell model can be replaced with more general non-linear stress-strain relations; like Avalle [24], or Liu-Subhash [23] have integrated in their models.

In the study of Liu and Subhash [23] a nonlinear phenomenological constitutive model is proposed. This model is intended for structural foams subjected to large deformations. To capture the hardening effect of materials, functions of the form $\sigma=A\varepsilon^{n}$ can be used, which is an exponential function continuously defined from 0 to $+\infty$. A and n are constants and ε is the strain. As originally described, the function could not capture the rapid densification phase during compression. To capture this phenomenon, an additional term was added. As a result, the function in its final form (Equation 2) can describe both the compressive and tensile responses of the material.

$$\sigma = A\frac{e^{\alpha\varepsilon}+1}{B+e^{\beta\varepsilon}}+e^{c}(e^{\gamma\varepsilon}-1) \quad \text{(Equation 2)}$$

Parameters A, B, α and β are constants, defined by the initial density and strain rate. Parameter C will stretch or shrink the curve on the strain axis without altering the origin of the plot. Additionally the term $e^{\gamma\varepsilon}$ allows the rapid increase in the stress value during densification to be captured. The Liu and Subhash constitutive model has mainly been developed to capture the fundamental stress-strain response in crushable foams subjected to large deformations. In the tests executed by Liu and Subhash [23], the model was applied to capture the stress-strain response of two structural foams when subjected to uniaxial compression. Macroscopic fracture for unconfined specimens occurred for strains less than 15% while confined specimens exhibit significantly larger strains extending beyond 50%. However, the quality of the strain measurement was questionable. In our experimental results, the deformations are very small, and the maximal failure strain is around 2%. Therefore, a model intended for large deformations will not accurately predict the stress strain relations of EPS foam at high strain rates.

In the study of M. Avalle [24], a new model was proposed describing the mechanical behavior of the cellular materials and enabling to account for the density dependency of the foam behavior. It is a micro-mechanical model and the density dependence laws are derived directly from micro-structural considerations and micro-mechanisms of deformation. The model has five parameters ((Equation 3). The parameters E, A and B are density dependent, while m and n are not. The first term fits the elastic and plateau region, while the second one fits the densification region

$$\sigma(\varepsilon) = A\left(1 - e^{-\left(\frac{E}{A}\right)\varepsilon(1-\varepsilon)^m}\right) + B\left(\frac{\varepsilon}{1-\varepsilon}\right)^n \quad \text{(Equation 3)}$$

Although this model describes the stress-strain curve of polymeric foams well, it does not include the effect of strain rate due to dynamic loading. A. Nagy [25] proposed a constitutive model including the strain rate effect described by a shape function. A new strain rate function ((Equation 4) was introduced by Y. Jeong [20] that describes the log-log plot of stress versus strain rate, which is concave up, at constant strain.

$$M(\varepsilon, \dot{\varepsilon}) = 1 + (a + b\varepsilon)\ln\left(\frac{\dot{\varepsilon}}{\varepsilon_0}\right) \quad \text{(Equation 4)}$$

The final form of the Avalle function where strain rate effects due to dynamic loading are taken into account can be described by (Equation 5:

(Equation 5)

$$\sigma = \left(A\left(1 - e^{-\left(\frac{E}{A}\right)\varepsilon(1-\varepsilon)^m}\right) + B\left(\frac{\varepsilon}{1-\varepsilon}\right)^n\right)\left(1 + (a + b\varepsilon)\ln\left(\frac{\dot{\varepsilon}}{\dot{\varepsilon_0}}\right)\right)$$

The five parameters, E, A, B, m, and n, are determined by fitting the experimental stress-strain data at the reference strain rate $\dot{\varepsilon}_0$. The remaining two parameters, a and b, are found by linearly approximating the experimental stress-strain data for another strain rate. The second term of (Equation 5) describes the densification region that is typically present in compression stress-strain curves. Tensile stress-strain curves do not have this region. In tension, the cell walls of the foam will be stretched and rupture, instead of the collapse and densification observed in compression loading. Therefore, the second term (with parameters B and n) can be left out when modelling tensile curves. The equation can then be simplified to:

(Equation 6)

$$\sigma = A\left(1 - e^{-\left(\frac{E}{A}\right)\varepsilon(1-\varepsilon)^m}\right)\left(1 + (a + b\varepsilon)\ln\left(\frac{\dot{\varepsilon}}{\dot{\varepsilon_0}}\right)\right)$$

where the parameters are dependent on the material density, and temperature [20]

Constitutive models are often used in FEA packages for material behavior simulations. Different models are available in commercial software like LS-Dyna from which the user can chose the one that best fits his application. B. Croop [10] used the material model of Low Density Foam (57#), Crushable Foam (63#), Fu Chang (83#), Modified Crushable Foam (163#) to calibrate and reproduce the behavior of polymeric foams. As EPS exhibits strain rate dependency in testing, a material model that accurately describes this strain rate effect must be used in FE simulations. The Modified Crushable Foam (163#) model failed to recreate the unloading behavior of EPS. Crushable Foam (63#) gave the best fit with experimental data for compressive loading, and was used for EPS core modeling [10]. For dynamic loading, dynamic material parameters need to be defined within these models for reliably modeling the EPS performance. However, due to the typical applications of foam materials, research efforts related to the proposed models are limited to compression loading. Validation of these models in tension for different ranges of strain rates and densities is something that has not been studied yet.

Tensile tests on EPS samples have been conducted by few researches so far and in densities and strain rates that are lower than what is expected in crush applications. C. Wensu [11] performed quasi-static tensile tests on low density EPS specimens of 13.5 kg/m³ and 28 kg/m³. A relation between tensile strength and density was found leading to increased strength when the density increases. According to Wensu this is due to the larger number of cells in the cross section that contribute to the strength of the material. The elasticity modulus in tension was found to be larger than in compression even though it was expected to be identical. This could be due to the non-linear material behaviour, and the determination of the end of the elastic region is difficult to define. Y. Gnip [4], performed tensile tests on EPS-foam according to the EN1607 standard, which mandates a load applied perpendicular to the cross section of the test specimen. Three test specimens were tested with thicknesses of 50mm, 100mm and 150mm and all with a density of 19.5 kg/m³. The stress-strain curves are quasi-linear at a strain below 2%. A. Pellegrino [5] studied the mechanical response of a syntactic polyurethane foam at low and high strain rates ($10^{-3}\ to\ 280\ s^{-1}$). This study also concluded that the tensile strength increases with increasing strain rate while the failure strain decreases.

T. R. Walter [6] studied the trend of the tensile E-modulus and the ultimate tensile stress as function of density. Both modulus and tensile stress increase with density of foam. A. Lorna [3] predicted that Young's modulus should increase with density in the elastic region as predicted by (Equation 7

$$E = E_s C_1 \left(\frac{\rho}{\rho_c}\right)^2 \qquad \text{(Equation 7)}$$

where subscript s refers to the full density solid and C_1 is an empirically determined constant.

The disadvantage of dynamic testing is the influence of inertial forces on the results at high strain rates. This is because an acceleration occurs at higher speeds, causing relatively high inertia forces. Important is that the acceleration can result in a non-constant strain rate during the experiment. At high strain rates, fractures are more likely to occur at the gripping point of the test specimens. The gripping of the specimens must therefore be done carefully and adaptively during dynamic tensile testing. In general, enough dynamic tests must be performed to acquire the dynamic tensile strength as well as possible. The testing machines, used in the experimental tests, measure displacements using either LVDT-sensors, extensometers and/or laser sensors. Extensometers can only be used in quasi-static tests at low speed. Also, LVDT's are often not linear throughout their range. The crosshead displacement is instead used to calculate the strain which offers

poor accuracy even at low loads. On the contrary, errors in displacement measurement are negligible in compression due to the long plateau region that is not observed in tension. To tackle this, DIC (Digital Image Correlation) has been suggested as an accurate method of measuring strains [15][14]. H. Koerber [16] used DIC for quasi-static and high strain rate experiments in order to obtain the in-plane strain field over the entire specimen surface. C. Ling [17] used DIC for the determination of the strain field of foam materials under combined compression-shear loadings while S. Hensley [18] used it for compression and bending experiments of foams materials in biomedical applications. S. Koumlis[28] used the technique to extract a nonlinear Poisson's ratio as a function of strain of open cell polyurethane foams.

In this article a systematic approach is followed to generate a wide range of data for the tensile properties of expanded polystyrene foam for which the information in literature is scarce. A detailed library of experimental data for different strain rates and densities was created and analysed. In contrast with the processes followed in the existing literature, an improved experimental approach was followed incorporating DIC for accurate strain measurements. The predictive capability of different constitutive models on foam materials was finally investigated based on the experimental data that were generated.

2. Experimental work

2.1. Test specimens

The tensile specimens were designed based on the guidelines given in ASTM: D3574 E, which stipulates the requirements for the tensile testing of foams. To meet the specific dimensions of the specimen's mold but also the specific production characteristics of the EPS used, the specimens needed to be customized and the dimensions were adjusted. The specimen gauge length was shortened. ISO 1926 [12] and ASTM D638 [13] suggest samples of 10 and 14 mm thickness respectively, ASTM D3574 E sets 30mm as minimum specimen thickness. In tensile testing, the scale of inhomogeneity of the material has to be significantly smaller than the dimensions of the specimen. The average EPS bead size ranges from 2.5 to 3 mm for the 80-120 g/l specimens and 3.4-5.5 mm for 60 g/l as presented in next chapter. This is only marginally smaller than a specimen of 10 -14 mm thickness. Therefore, the specimens were created with a thickness of 30 mm, that is

significantly greater than the size of the beads, and a length of 80 mm.(Figure 1). For the fixation of the specimens on the set-up, clamping the foam in the grips would lead to crushing, large deformations and densification, while avoiding the crush region would reduce the clamping force, making it impossible to avoid slip. Therefore, an alternative clamping method was used. The test specimens were adhesively bonded to a T-shaped steel gripping piece as is described later on. The large contact surface between the steel and the foam allowed the adhesive to effectively transmit the forces to the test specimen. Four different densities of the same foam-type (EPS) tested; 60, 80, 100 and 120 g/l.

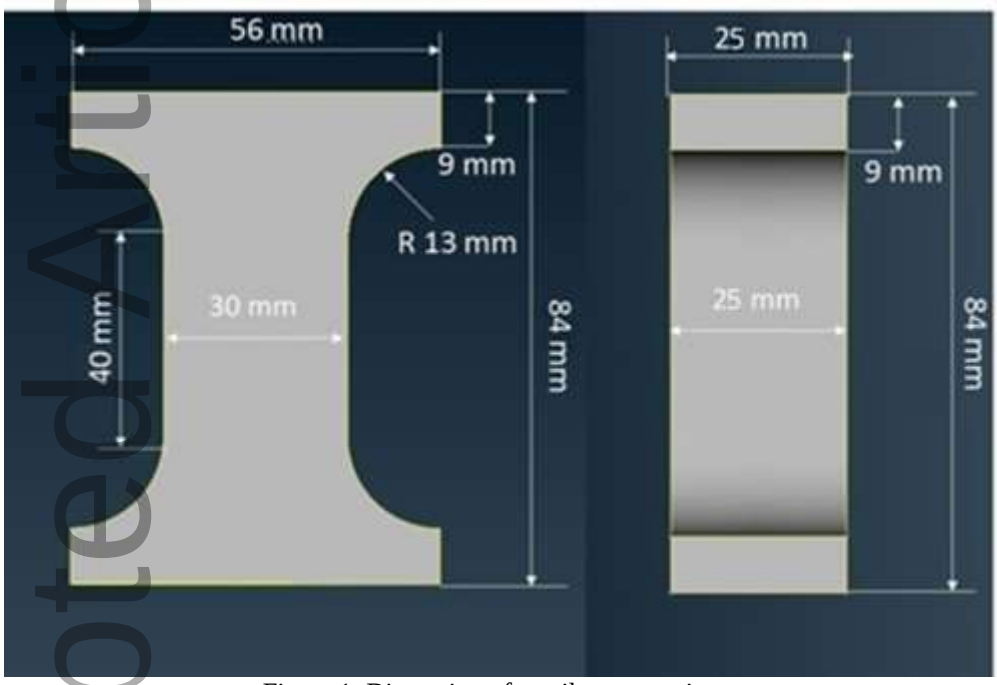

Figure 1: Dimension of tensile test specimen

2.2. Testing facilities and setup

Because of the range of speeds that needed to be tested, different testing machines have been used to test the specimen. At low strain rates standard quasi-static testing machines (Instron 4467, 5567) were used, while at medium strain rate, the dynamic testing machine (Instron 8502) was more suitable. For high strain rates, the standard High-Speed test machine (Instron 8502) could not reach the high displacement rates needed. Therefore, an alternative method was developed. The frame of the shear impactor, as presented in the study of C. Ling [17], originally used to test EPS foam under combined compression-shear loading, was modified to perform tensile tests. The modified impact tester (Figure 2) consists of:

- Frame that holds the falling mass mechanism (height is adjustable)
- Piezo-electric load cell (50 kN) with suitable charge amplifier (Kistler, type 5007)

- Laser sensor MEL25, 100 mm range, 25 kHz bandwidth

- Simultaneous sampling of force and displacement at 200kHz

-DIC equipment for strain measurement on the specimen, as presented in following chapter

The main aim is to convert the kinetic energy of the mass in free fall to the required energy for breaking the test specimen. To avoid significant reduction of the strain rate during the test, the impact energy should largely exceed the fracture energy of the test specimen. Two methods of load transfer from the falling weight to the test specimen were considered, an impact system or a pulley system. The disadvantage of a pulley-system is that it does not offer a compact solution and additional parts and assemblies needed to be installed on the impact tester. The slinging of the cable would also be difficult to control when the mass would be in free fall. The cable can also be stretched and deformed; therefore there would be a difference in speed between the free-falling mass and the specimen. These sources of variance could be better controlled by the use of a thicker cable but that would add more weight and reduce the agility of the rope. The impact system (Figure 2) can however just be placed at the bottom of the impact tester, without modifying the impact tester itself. Therefore, the impact system was chosen. The impact tester uses two steel cylinders as a guide for the mass to fall in a stable manner and to hold the mass at an adjustable height. Both a magnetic lock and a manual lock are used as safety measures.

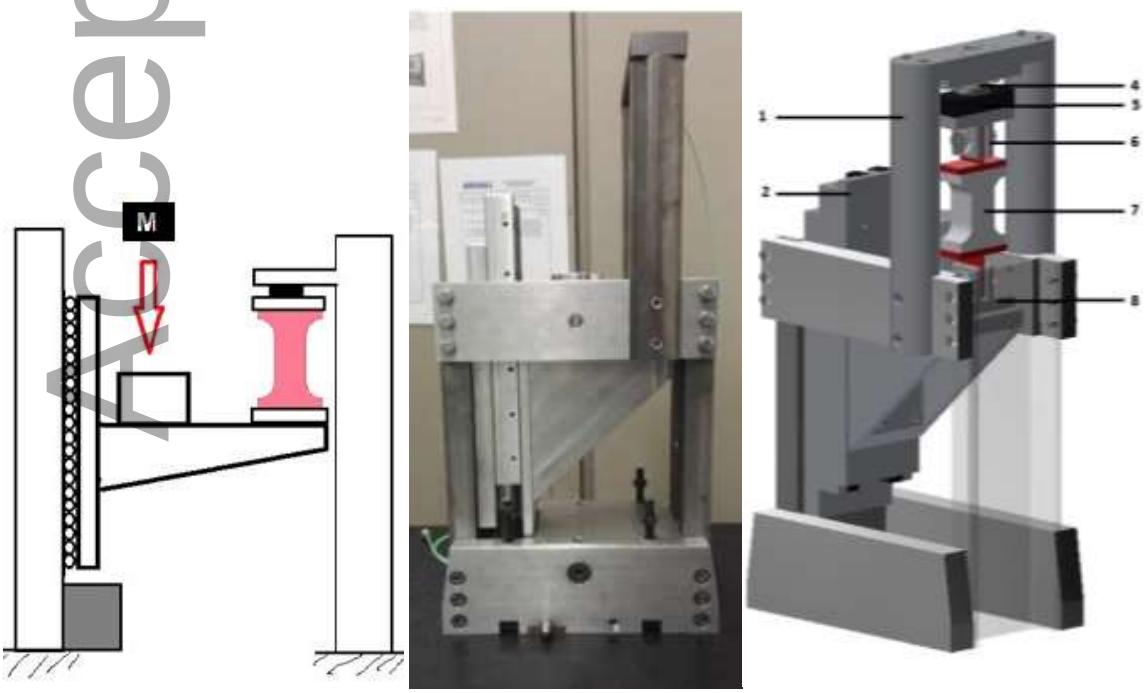

Figure 2: Raw sketch and functioning principle and final result of drop-weight impact system for tensile tests

Table 1: Testing machines used for different strain rates and measured strain rates

Test machine	**Speed**	**Input speed**	**Target Strain Rate (s^{-1})**	**Average Measured Strain Rate (s^{-1})**
Instron 4467/5567	Low	10 mm/min	0,003	0,003
Instron 4467/5567	Low	250 mm/min	0,06	0,053
Instron 8502	Medium	0,1 m/s	1,5	1,405
Drop weight impact	High	1,2 m/s	30	27,0
Drop weight impact	High	2,4 m/s	60	59,3

The target (nominal) strain rates and the corresponding speed of the testing machine or drop weight are shown in Table 1. To explore the strain rate dependency of the tensile properties, it was opted to use the average strain rate across all specimens tested at one specific machine setting. ANOVA test was performed to evaluate the statistical difference between measured strain rates per density. A p-value<0.05 was chosen to identify statistical significance. Further details are presented in the following chapters

The drop weight system (Figure 2) consists of a linear motion rail (2) that allows vertical displacement after impact. The rail is connected to the impact-block (3) and the lower specimen grip (8). When the impact block (3) is hit by a falling impact weight, the load and energy of the impact is transferred via the lower grip (8) to the test specimen (7). The specimen is attached to the impact block by the lower grip (8). The upper side of the test specimen is clamped by the upper grip (6) that is connected to a rigid frame (1) by a tension plate (5) and the load cell (4). The guide used is a frictionless motion table NK6-310 manufactured by Schneeberger. The desired velocities are attained by dropping a mass from variable heights and are calculated with the equations of a falling body

$$V = \sqrt{2gd} \qquad \text{(Equation 8)}$$

where V the instantaneous velocity, d the distance travelled and g the gravitational acceleration. The weight used for the impact was a 5 kg steel plate.

The maximum height (d) of the set is 0,8 m which corresponds to a velocity of 3,96 m/s. The corresponding velocities to the tested strain rates of 30 s^{-1} and 60 s^{-1} are 1,2 m/s (3,6 J) and 2,4 m/s (14,4 J) which are within the functional limits of the drop tower (Table 1) To avoid significant reduction of the strain rate during the test, the impact energy should largely exceed the fracture energy of the test specimen. Assuming a brittle material (foam) the fracture energy can be estimated with the equation below

$$U_{fracture} = 0{,}5*V*UTS*\varepsilon_f \quad \text{(Equation 9)}$$

where UTS is the Ultimate Tensile Strength, V is the volume of the sample and ε_f the strain to failure of the material. Assuming UTS of 1,5 MPa, strain to failure ε_f of 1,5 % and a volume of sample V of 30.000 mm^3, the fracture energy can be estimated to 0.33 J which is significant lower than the impact energy

For gripping the specimens, direct loading of the foam should be avoided: wedge grips result in significant compressive stresses and considering the magnitude of the clamping force with respect to the compressive strength of the foam, this might result in compressive failure in the grips. Therefore, a T-shaped metal gripping piece was created. (Figure 3) The part is adhesively bonded to the foam, while the vertical flange of the T-piece can be gripped in standard wedge clamps. Thus, direct loading of the foam in the grips is avoided, and load transfer is achieved with minimal stress concentration, provided that bending moments due to asymmetric clamping can be avoided. The grips were glued onto the specimens. The adhesive used was a two-component epoxy adhesive (AW 106 Resin/Hardener HV 953).

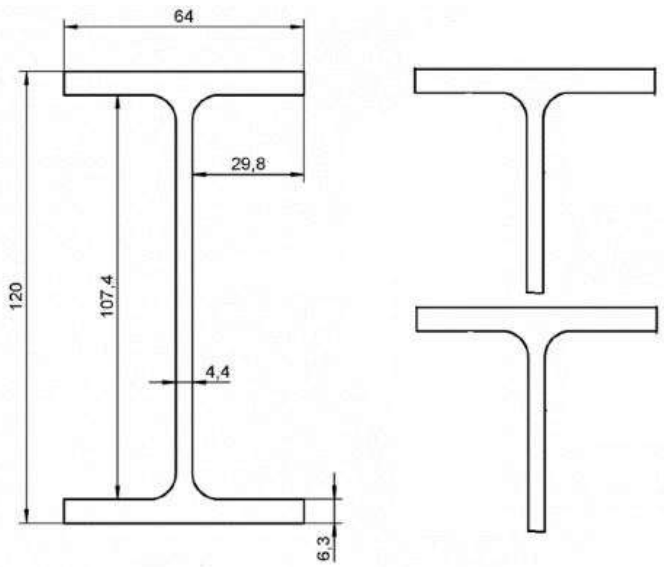

Figure 3: IPE 120 beam cut in two pieces

2.3. Tensile experiments

For every parameter combination (density and speed), three specimens are tested to account for variation in the results. As also stated in ASTM D1623, defective specimens that would break at some obvious macroscopic flaw are to be discarded and retested, unless such flaws constitute a variable that is to be studied. Specimens that break in the gripping area were discarded as well. Five different strain rates were

tested (Table 1). The force is measured using the load cell on the machines, while the displacements are measured using digital image correlation based strain mapping.

To ensure that the specimen was tested in pure tension the steel T-profiles glued to the ends of the specimen should be aligned perfectly. This was ensured by defining the axis of symmetry of each specimen and placing the T shapes in a way that their centers would always coincide with the axis of the specimen.(Figure 4)

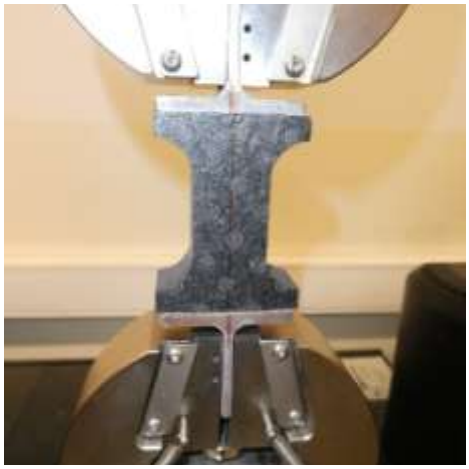

Figure 4: Indicative alignment of specimen with T-Shapes

During preliminary tests on the drop tower, force oscillations were observed in the load measurements. Those oscillation could be caused by two different mechanisms. The first mechanism is a result of the inertial forces due to the high speed impact of the mass colliding with the impact-block. The impact of the two metals causes vibrations that are detected and measured by the load cell. To eliminate these oscillations two approaches were investigated for densities 80 and 100 g/l according to the availability of samples. In the first approach the oscillations were damped out by using a rubber damper between the two colliding metals while in the second approach a Fourier transform and a low-pass filter was applied on the force-time curves. The second mechanism is a result of the internal defects in the material (i.e. internal porosity from production), which fail internally and cause the specimen to fracture. In this case, the fluctuations are inherent to the material behavior.

2.4. Measurement of strains

The testing machines, used in the experimental tests, measure the displacements using either LVDT-sensors, extensometers and/or laser sensors. Extensometers can only be used in quasi-static tests at low

speed, while at medium and high speeds (dynamic testing) the use of extensometers is impractical or even impossible. For that reason DIC (Digital Image Correlation) was used for the measurement of strains using a Photron FASTCAM Mini AX100 high speed camera. The working principle of DIC is that there is a direct correspondence between the motions of points in the image and motions of points on the object. For the technique to work effectively the pixel blocks need to be random and unique with a range of contrast and intensity levels.[26]

The velocity of the sample's moving head, corresponding to each engineering strain rate (Table 1) was calculated in advance, before the experiments. For experiments in low strain rates that were conducted with the Instron testing machines, the velocity was used as an input for the machine's moving head. For experiments in high strain rates that were conducted with the modified set-up, the velocity was used as input for the dropping height. In both cases the velocity of the sample's moving head was cross verified through DIC (last column table 1).

To capture the deformations of the specimen at different strain rates, the frame rates and resolution of the camera was changed accordingly. The camera settings are shown in Table 2. In the first row, the target strain rates for which the testing rigs were set, are presented.

Table 2: Frame rate and resolution settings at various target strain rates

Strain rate (s^{-1})	**Frame rate (fps)**	**Resolution**
0,003	125	1024x1024
0,06	250	1024x1024
1,5	4000	1024x1024
30	50000	256x125
60	50000	256x125

The HS camera is set up in line and at the same height as the specimen. For the analysis VIC-2D was used as compatible with FASTCAM Mini AX100 camera. For computing the engineering strain, a reference image taken while no load was applied. VIC-2D will then compute the displacements of all images with respect to this reference image. When the reference image is set, the subset and the step size can be selected.(Figure 5)

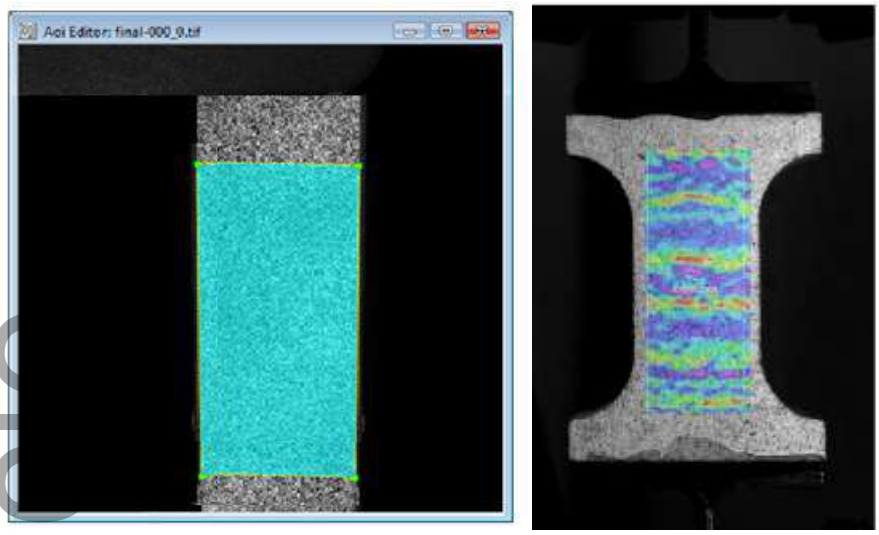

Figure 5: Selecting a rectangular AOI (Area-of-interest) and example of visualization of results on specimen

The step size controls the spacing between the points that are analyzed during correlation. A step size of 1 corresponds to a correlation executed at every pixel inside the area-of-interest. The analysis time increases as the step size is decreased. The subset size is an area manually selected and it controls a particular area of the image that is used to calculate the displacement between images. It has to be large enough in order to include a sufficiently distinctive pattern in the area used for correlation. The larger the subsets, the better the results. It is important that the subset size is chosen in accordance with the expected deformations. Correlation starts from Seed Point (SP) which is best if it is a point with the minimum displacement during the test. For instance, if a specimen is tested in a tensile frame, the seed point should be placed as close to the stationary grip as possible. The set up arrangement used is shown in Figure 6

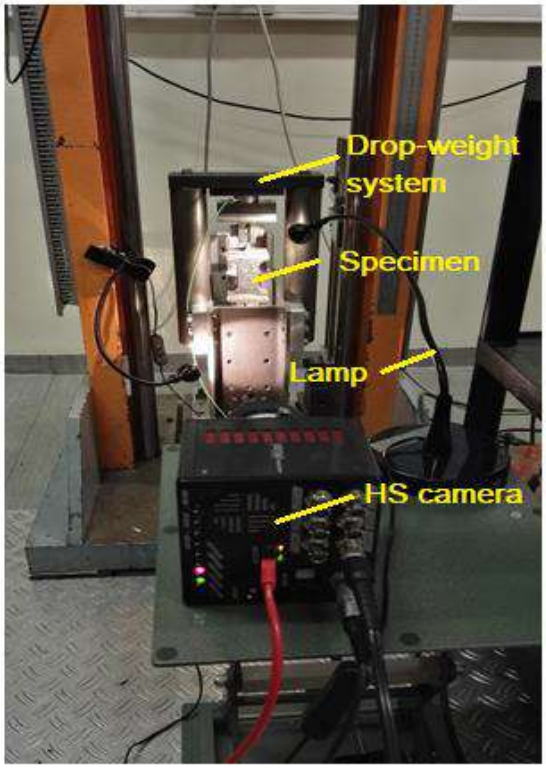

Figure 6: Setup of HS camera in front of testing machine

3. Results

3.1. Presentation of results

For every density and strain rate, a minimum of 3 specimens have been tested. Unlike several results in literature, there is no significant delay in the build-up of stress in the stress-strain curve. However, at higher strain rates, some waviness in the curves is still present, most likely related to impact vibrations. Nevertheless, several observations can be made. [29].

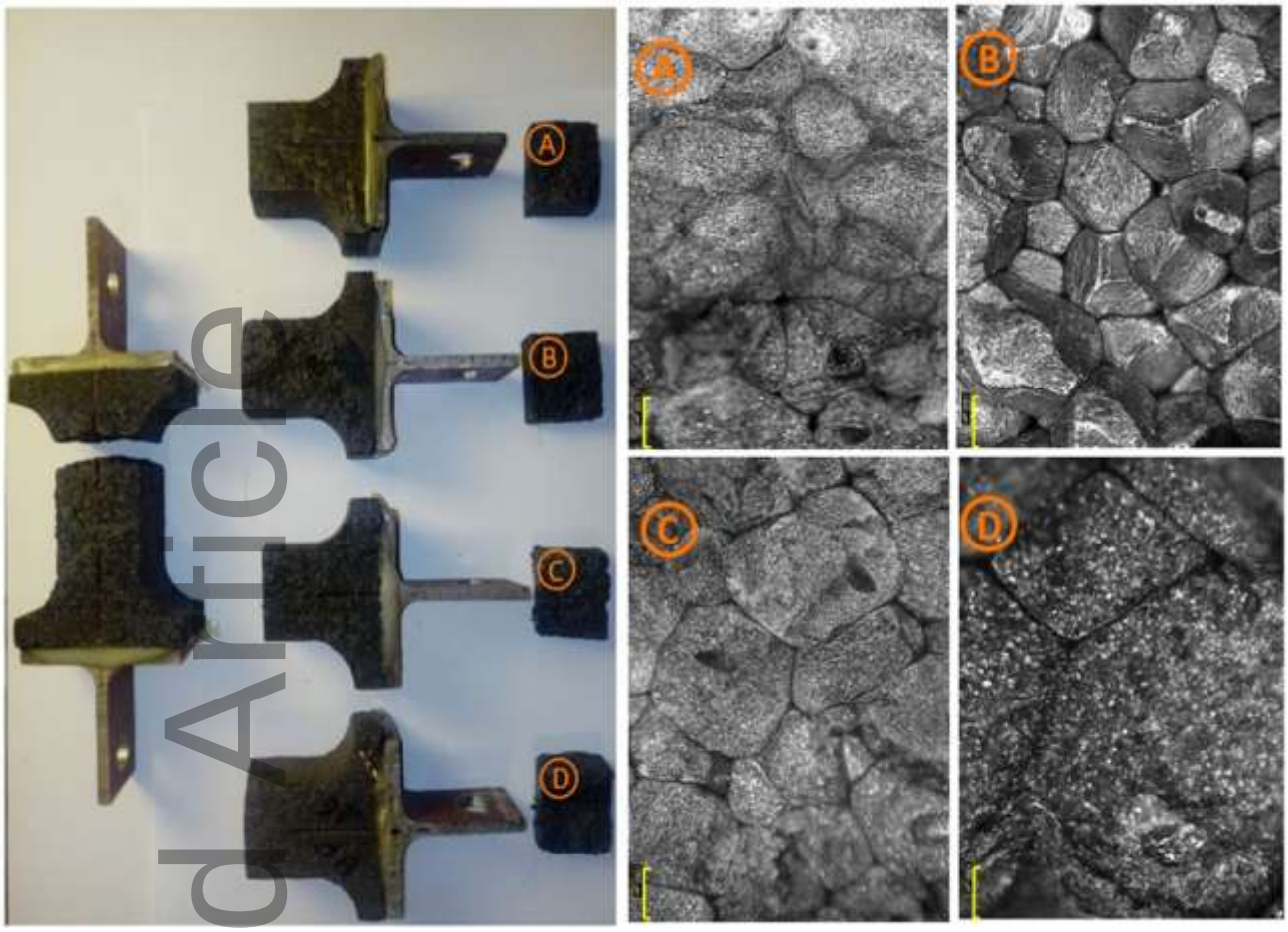

Figure 7: Fractured samples and stereo microscopy of top view of cross section per density From Upper to lower A:120, B:100, C:80 and: D:60 g/l. The lines on the stereo microscopes correspond to a length of 1000μm

An increase in the tensile strength is observed when the strain rate increases in addition to a decrease of the failure strain with increasing strain rate. As already mentioned in the previous chapter, to reduce force oscillations in measurements when using the drop-weight, two approaches were investigated aiming at the elimination of inertial forces due to the high speed impact of the mass colliding with the impact-block. The impact of the two masses causes vibrations that are measured by the load cell. These vibrations were damped out by using a rubber damper between the two colliding metals (densities 80 and 100 g/l) or by filtering out the oscillations (all densities). The two approaches produce curves with less oscillations and as a result a lower UTS due to their elimination. A representative comparison between the different solutions is shown in Figure 8 for 80 g/l and strain rate of 30 s^{-1}

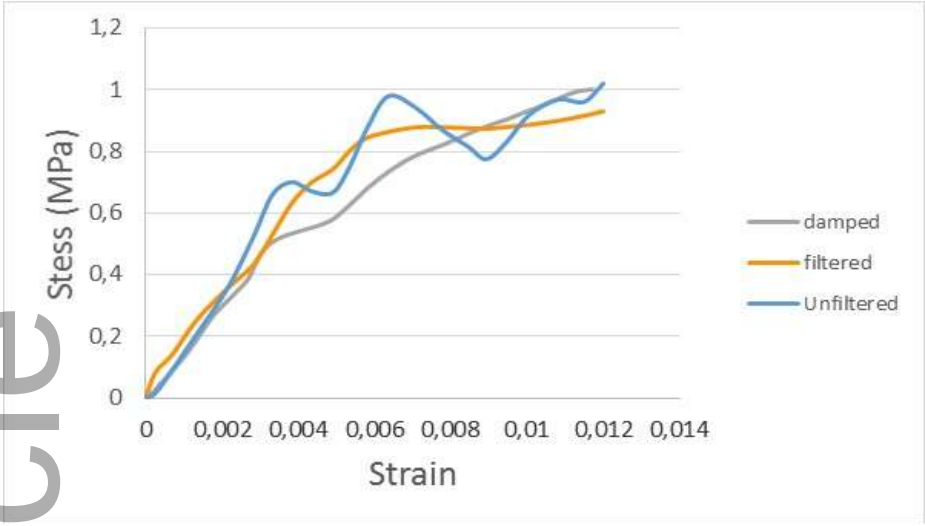

Figure 8: Representative comparison between damping solution and filtered results for 80 g/l

The summarized results for Strain to failure and UTS, for each strain rate and density are shown in Figure 9 and Figure 10 respectively. Each point of the graphs represents the average of each set of experiments. The results are plotted in a logarithmic scale on the horizontal axis. The trendlines of the graph for strain to failure versus strain rate show a decrease of the strain to failure with increasing strain rate. When density is increased the strain to failure also decreases. The strain rate sensitivity of the strain to failure decreases with increasing foam density. It can be concluded that the strain rate dependency of the strain can be approximated as logarithmic: $\varepsilon = A.ln(\dot{\varepsilon}) + B$ where $\dot{\varepsilon}$ is the strain rate.

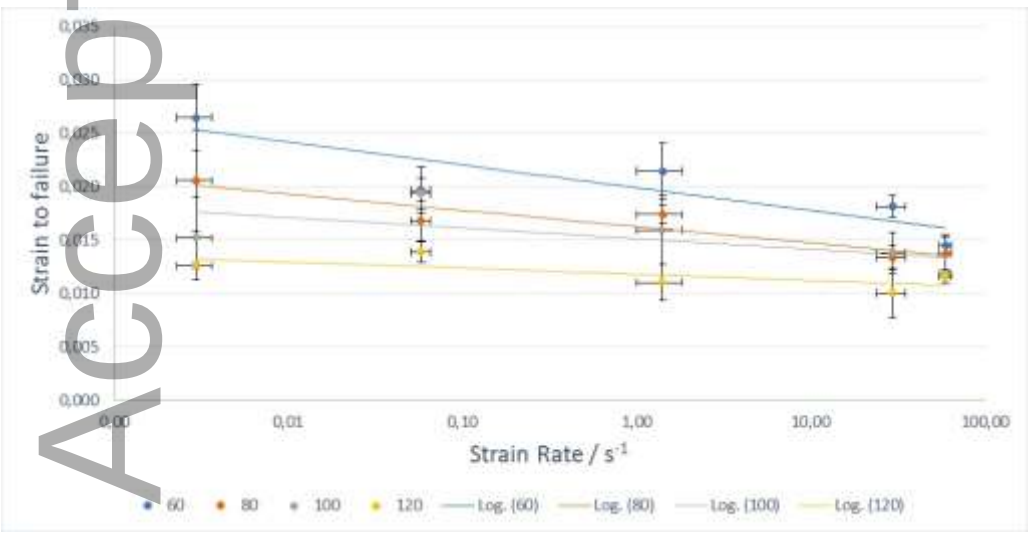

Figure 9: Strain to failure per strain rate and EPS density. The vertical error bars represent the standard deviation of the Strain to failure and the horizontal the standard deviation of the strain rate

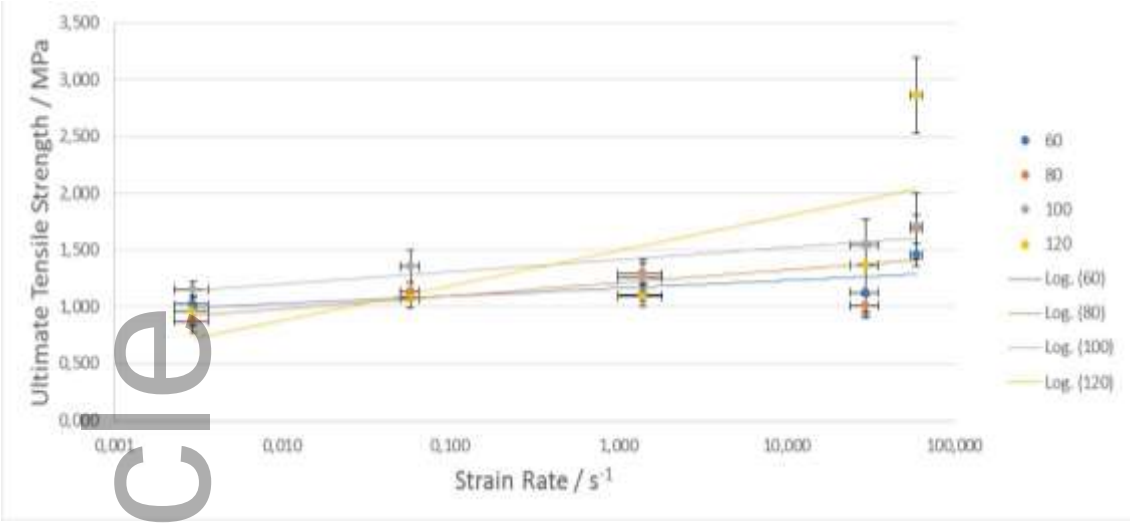

Figure 10: UTS per strain rate and EPS density. The vertical error bars represent the standard deviation of the Strain to failure and the horizontal the standard deviation of the strain rate

The corresponding values of A and B and the accuracy of fitting for each density are shown in Table 3

Table 3: Curve fitting coefficients for Strain to failure

	$A_{Strain\ to\ failure}$	$B_{Strain\ to\ failure}$	R^2 value
60 g/l	-0,0009	0,0201	0,76
80 g/l	-0,0006	0,0162	0,86
100 g/l	-0,0004	0,0153	0,43
120 g/l	-0,0002	0,0118	0,51

The logarithmic trendlines for UTS also show a general trend towards an increase of the tensile strength with increasing strain rate. However due to the scatter on the individual test data it is more difficult to see a clear trend, a possible outlier for the highest strain rate of 120 g/l can be observed. The curve fitting coefficients for UTS as a function of strain rate are shown in Table 4

Table 4: Curve fitting coefficients for UTS

	A_{UTS}	B_{UTS}	R^2 value
60 g/l	0,030	1,166	0,69
80 g/l	0,049	1,219	0,46
100 g/l	0,058	1,419	0,75
120 g/l	0,135	1,497	0,55

Figure 11 presents the UTS as a function of the foam density for different strain rates. The increase in UTS is less pronounced for low strain rates.. At higher strain rates (30 and 60 s^{-1}), the UTS does show the expected increase as a function of the foam density. The highest strain rate dependency is observed for 120 g/l followed by the 60 g/l

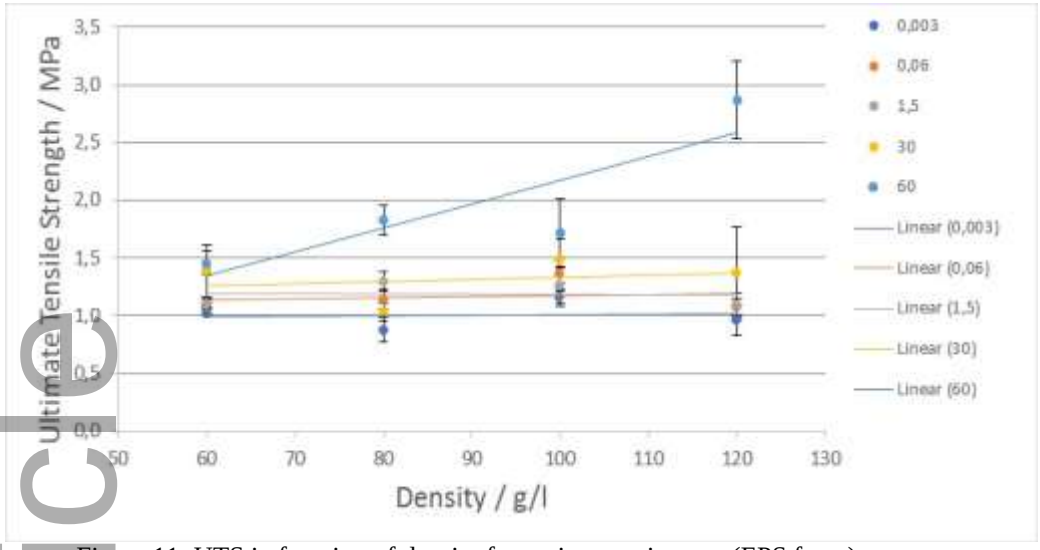

Figure 11: UTS in function of density for various strain rates (EPS foam)

The results of the tensile properties for different strain rates and densities are summarized in Table 5. During measurements, some variance was expected from the nominal values of the strain rates. as a result of slippage, the machine's annotations and varying crosshead displacement rates. The standard deviation and average value per strain rate are presented in table 5. Results of the statistical analysis showed no statistical difference between the measured strain rates per target rate. (p-values: 0.065, 0.658, 0.182, 0.106 and 0.22 for target strain rate 0.003 $\mathbf{s^{-1}}$, 0.06 $\mathbf{s^{-1}}$, 1.5 $\mathbf{s^{-1}}$, 30 $\mathbf{s^{-1}}$ and 60 $\mathbf{s^{-1}}$ respectively)

Table 5: Tensile properties (UTS, Elastic Modulus and Strain to failure) in function with density and strain rate

		Nominal Strain Rate	**0.003**	**0.06**	**1.5**	**30**	**60**
	Strain rate (s^{-1})	**Average Strain Rate**	**0,003**	**0,053**	**1,405**	**27,036**	**59,339**
		$S.DEV_{S.R}$	**0,001**	**0,013**	**0,412**	**1,669**	**4,498**
Density (g/l)	**60**	**UTS (MPa)**	1.02	1.009	1.10	1,38	1,45
		$S.DEV_{UTS}$	0,011	0,015	0,04	0,3	0,12
		Failure Strain	0.0265	0.0197	0.0215	0.0185	0,0145
		$S.DEV_{strain}$	0,003	0,002	0,003	0,001	0,001
		Modulus (MPa)	58,3	51,4	69,1	102,7	127,0
		$S.DEV_{Young}$	0,500	0,530	0,190	3,9	6,5
	80	**UTS (MPa)**	0.88	1.14	1.29	0,95	1,83
		$S.DEV_{UTS}$	0,1	0,08	0,09	0,1	0,13
		Failure Strain	0.0206	0.0168	0.0174	0.0131	0,0137
		$S.DEV_{strain}$	0,005	0,002	0,001	0,001	0,002
		Modulus (MPa)	71,5	62,6	67,5	108,1	141,7
		$S.DEV_{Young}$	9,3	23,6	2,3	3,3	16.0
	100	**UTS (MPa)**	1.16	1.36	1.25	1.47	1,71
		$S.DEV_{UTS}$	0,07	0,04	0,16	0,2	0,29
		Failure Strain	0.0152	0.0194	0.0160	0.0138	0,0117
		$S.DEV_{strain}$	0,004	0,001	0,003	0,002	0,001
		Modulus (MPa)	108	62,8	102,5	139,2	155,7
		$S.DEV_{Young}$	6,5	6,1	23,8	33,2	15,0
	120	**UTS (MPa)**	0.96	1.07	1.09	1.36	2,86
		$S.DEV_{UTS}$	0,130	0,08	0,09	0,42	0,34
		Failure Strain	0.0122	0.0139	0.0110	0.0100	0,0116

		S.DEV$_{strain}$	0,001	0,001	0,002	0,002	0,001
		Modulus (MPa)	120,4	63,1	132,4	146,17	149,8
		S.DEV$_{Young}$	4,4	7,2	17,8	18,6	8,8

The Fracture energy as a function of the strain rate is plotted in Figure 12, calculated as the area under the stress-strain curves up until fracture. Results show a significant decrease of the fracture energy with increasing strain rate for the lowest density of 60 g/l, while for the other foam densities, the fracture energy remains constant. That is an important property for foams, as they are typically used for body protection at higher strain rates.

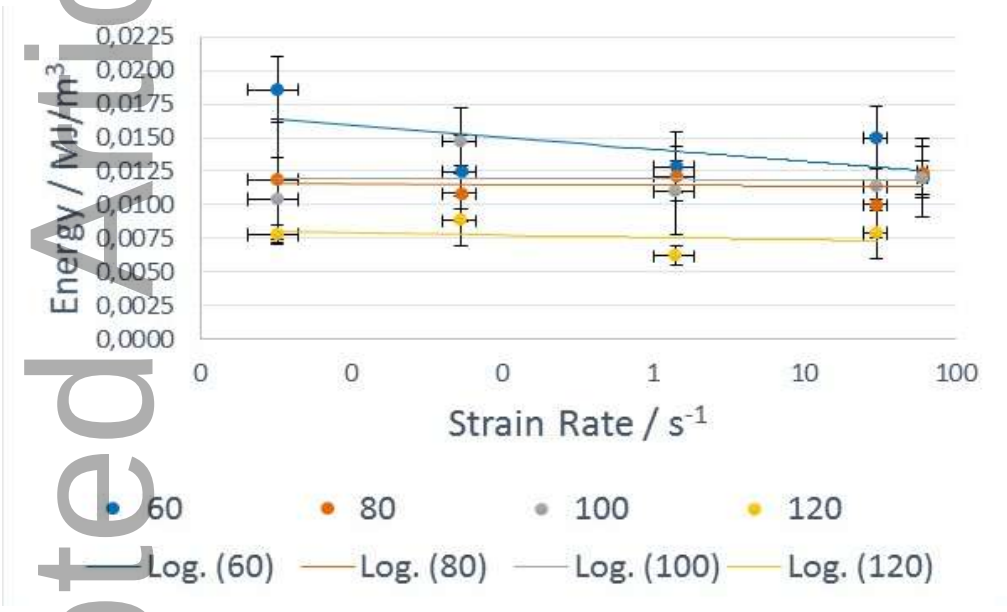

Figure 12: Fracture energy in function of strain rate for various strain rates of EPS foam

The elastic modulus as function of the strain rate is plotted in Figure 13. The elastic modulus was calculated at a strain below 0.2%, where the curves are approximated as linear elastic. Despite the small fluctuation of the modulus as function of strain rate, an increase as the strain rate increases is also observed here.

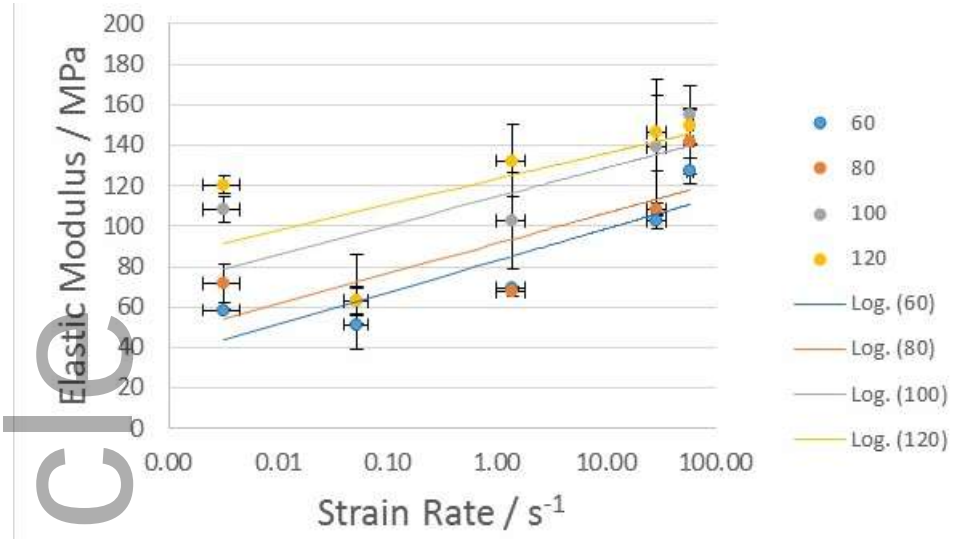

Figure 13: Elastic modulus in function of strain rate for various densities of EPS foam

Except at a strain rate of 0.06 s^{-1}, where the modulus decreases, the general trend does indeed show an increase and a linear proportionality between the modulus and the density, as stated in (Equation 7)

If we plot the modulus in function of density (Figure 14) we see an increase in the modulus as function of density. A reduction is noticed in the individual data for a strain rate of 60 s^{-1} and density above 100 g/l however the general trend does indeed show an increase and a linear proportionality between the modulus and the density, as already stated in (Equation 7.

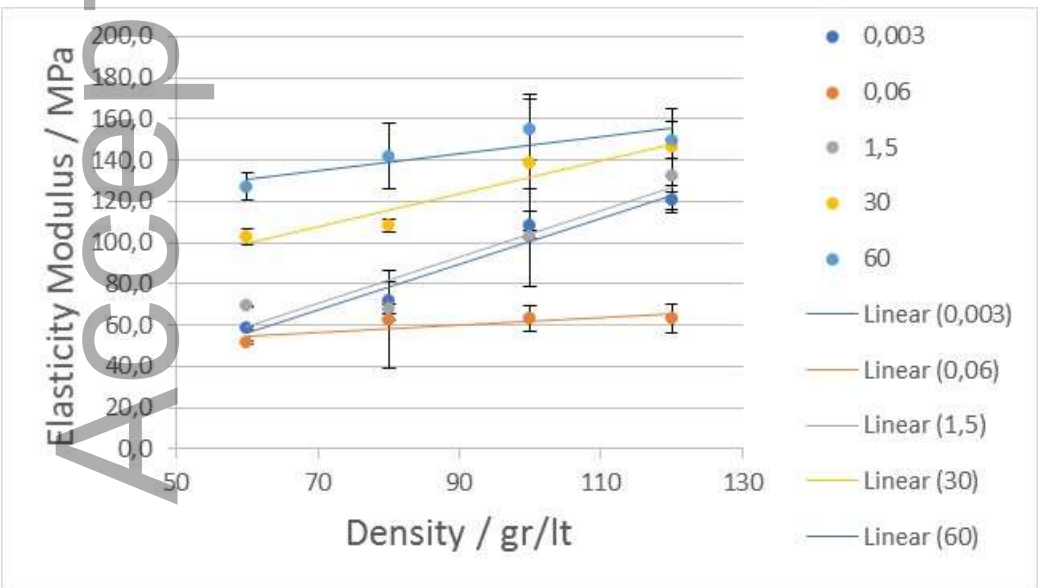

Figure 14: Elastic modulus in function of density for various strain rates (EPS foam)

The strain rate dependency of the tensile properties of EPS foam is shown in Figure 16 along with the curves predicted by the Avalle model through the process presented in the next chapter. Each curve

presented in the graph is the average of each set of curves created per density and strain rate as described above. To avoid statistical fluctuations from the measurements in the final curves, the strains plotted correspond to those calculated by the logarithmic functions of Table 3. The corresponding UTS result by extrapolating the averaged curves to the calculated strains. Out of the three possible sets of curves depending on the density (unfiltered, filtered, damped), the set that was finally selected, was the one with the best quality of fit to the Avalle model (Table 8-

Table *10*). In all cases, filtered or damped sets of curves resulted to the best fitting. The model and the calculation of the fitting quality is presented in the following chapter.

Several studies. [20][21][29][30] have shown that small details of the foam morphology, like cell irregularity, cell wall thickness variations, waviness, non-uniform cell wall thickness, cell-size variations, fractured cell walls, cell-wall misalignments, and missing cells (Figure 15) [21] strongly influence the mechanical responses Therefore, deviations in the results are due to the nature and irregularities of polymeric foams

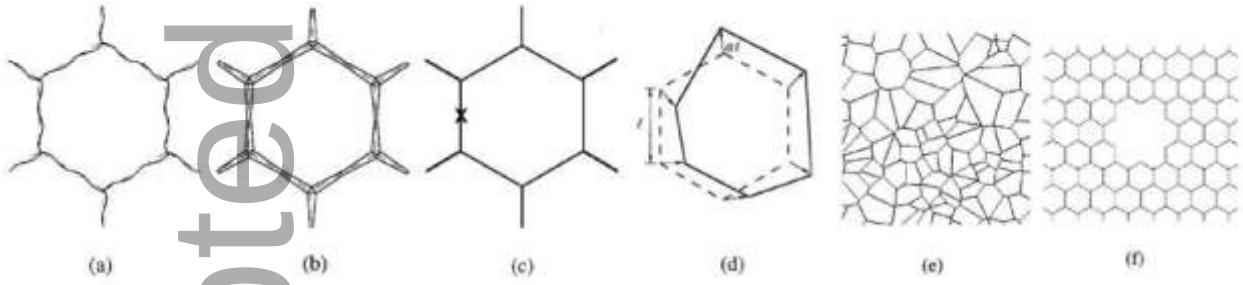

Figure 15: Six different types of geometric imperfections in foam materials (a) waviness; (b) non-uniform wall thickness; (c) fractured cell walls; (d) cell-wall misalignment; (e) Voronoi structure; and (f) missing cells. [21]

Such imperfections were indeed observed in the cell-size variation through stereo-microscopy conducted on the cross-section of the tested samples (Figure 7) for High testing speeds (HTS) (30-60 s^{-1}) and Low testing speeds (LTS) (0.003-1.5 s^{-1}). The beads´ size for density 60 g/l was on average bigger than the rest of the densities tested (LTS_{60}: 3.4 mm, HTS_{60}: 5,5 mm) that did not seem to differ much from each other ($LTS_{80\text{-}100}$: 2.5 mm, $HTS_{80\text{-}100}$: 3 mm)

Trans and intra bead fracture was observed in all cases (Figure 7) which is in agreement with the study of Mills and Kang[27]. Higher densities (80,100,120 g/l) were more prompted to fracture on the beads' boundary surface or close to it which was attributed to the strengthening caused by the increased bead

density. The presence of pores inside the bead was observed, in fracture surfaces of 80 and 100 g/l (Figure 7c). These larger pores reduce the local areal density and are likely to affect failure strength.

The measured dimensions of beads, are smaller in specimens tested at low speeds compared to those tested at high speeds, especially for 60 g/l. This could be indicative of a shift in the fracture type. At slow speeds, the fracture runs between the beads by a slow coalescence of interbead porosities. As a result, the top sides of the beads are mainly observed resulting to smaller average dimensions of beads. For high testing speeds, the fracture surface of 60 g/l seems to be almost pure intra-bead failure. Cutting across a bead will produce larger dimensions in the fracture surface..

As a result of the above observations, scatter should indeed be expected in the measured mechanical properties

However a full fractographic study was not performed since the present paper is mainly focused on the influence of macroscopic features on the fracture behavior, namely strain rate and density, without going into a microscopic level.

3.2. Model fitting to experimental data

For the reasons already mentioned in previous paragraph, the Avalle model (Equation 6) was chosen for validation and comparison of the experimental data. The model parameters are material, density and temperature dependent constants. Each of these constants changes an aspect of the shape of the final stress strain curve. These parameters can be determined by applying curve fitting of the theoretical equation of the model to the experimental data. To do so, the method of least squares was used of MATLAB's curve fitting toolbox. The proposed model of (Equation 6 has five parameters. Firstly, the three parameters, E, A, and m are determined by fitting the model to the experimental stress-strain curves at a "reference strain rate". Next, the remaining two parameters, a and b are found by linearly approximating the experimental curve at the remaining strain rates. To do so, it is important to define which strain rate from the experimental tests, should be set as the reference strain rate (ε_0). It is not obvious to pick one strain rate over the others. It is therefore best to estimate the parameters a and b for different reference strain rates and evaluate which provide the best results.

If a reference strain rate is defined, the term $ln\left(\dot{\varepsilon}/_{\dot{\varepsilon}_0}\right)$of (Equation 6 equals 0 and parameters a and b are omitted from the equation. Parameters E, A and m are calculated for that reference strain rate and afterwards parameters a and b, for each of the remaining strain rates. By calculating the variance, we can determine which reference strain rates provides the lowest variance. Table 6 indicatively illustrates the described working method as applied for EPS density 60 g/l. As can be seen in

Table 6, the variance for parameter b is high, showing that caution is necessary when interpreting these data.

Table 6: Parameter estimation of parameters a and b for different reference strain rates (density 60 g/l)

Reference strain rate ε_0	**0.003**		**0.06**		**1.5**		**30**		**60**	
Parameters	**a**	**b**	**a**	**b**	**a**	**b**	**a**	**b**	**a**	**b**
$\dot{\varepsilon}$= 0.003	-	-	0.016	0.478	-0.050	3.012	0.006	1.353	0.056	-0.110
0.06	-0.045	5.280	-	-	-0.071	1.942	0.021	0.431	0.088	-1.031
1.5	0.034	2.329	-0.086	3.260	-	-	0.096	-0.519	0.187	-2.570
30	0.001	2.481	0.133	-5.765	0.135	-0.964	-	-	0.724	-10.130
60	0.109	1.593	0.577	-19.530	0.470	-8.420	1.377	-27.440	-	-
Average	**0.007**	**2.921**	**0.160**	**-5.389**	**0.121**	**-1.108**	**0.375**	**-6.544**	**0.264**	**-3.460**
Variance	**0.004**	**1.97**	**0.064**	**77**	**0.05**	**20**	**0.3**	**146**	**0.07**	**16**

The strain rate that gave the least variance was 0.003s^{-1} thus that was the one selected as reference. The final values of each parameter for the Avalle model for each density are shown in Table 7

Table 7: Parameter estimation of E, A, m, a and b per density.

Density (g/l)	**E**	**A**	**m**	**a**	**b**
60	83.6	709700.4	27.9	0.007	2.9
80	80.4	709743.7	28.2	0.040	3.8
100	129.5	709752.4	35.7	0.010	2.1
120	111.1	709682.4	15.2	0.012	3.8

Indicatively for density 60 g/l, the constitutive equation can thus be written as follows bellow (Equation 10):

$$\sigma = \left(\mathbf{709700}\left(1 - e^{-\left(\frac{\mathbf{84}}{\mathbf{709700}}\right)\varepsilon(1-\varepsilon)^{\mathbf{28}}}\right)\right)\left(1 + (\mathbf{0.007} + \mathbf{2.9}\varepsilon)\ln\left(\frac{\dot{\varepsilon}}{\mathbf{0.003}}\right)\right) \quad \text{(Equation 10)}$$

The comparison of the model prediction and the experimental results are plotted in Figure 16.

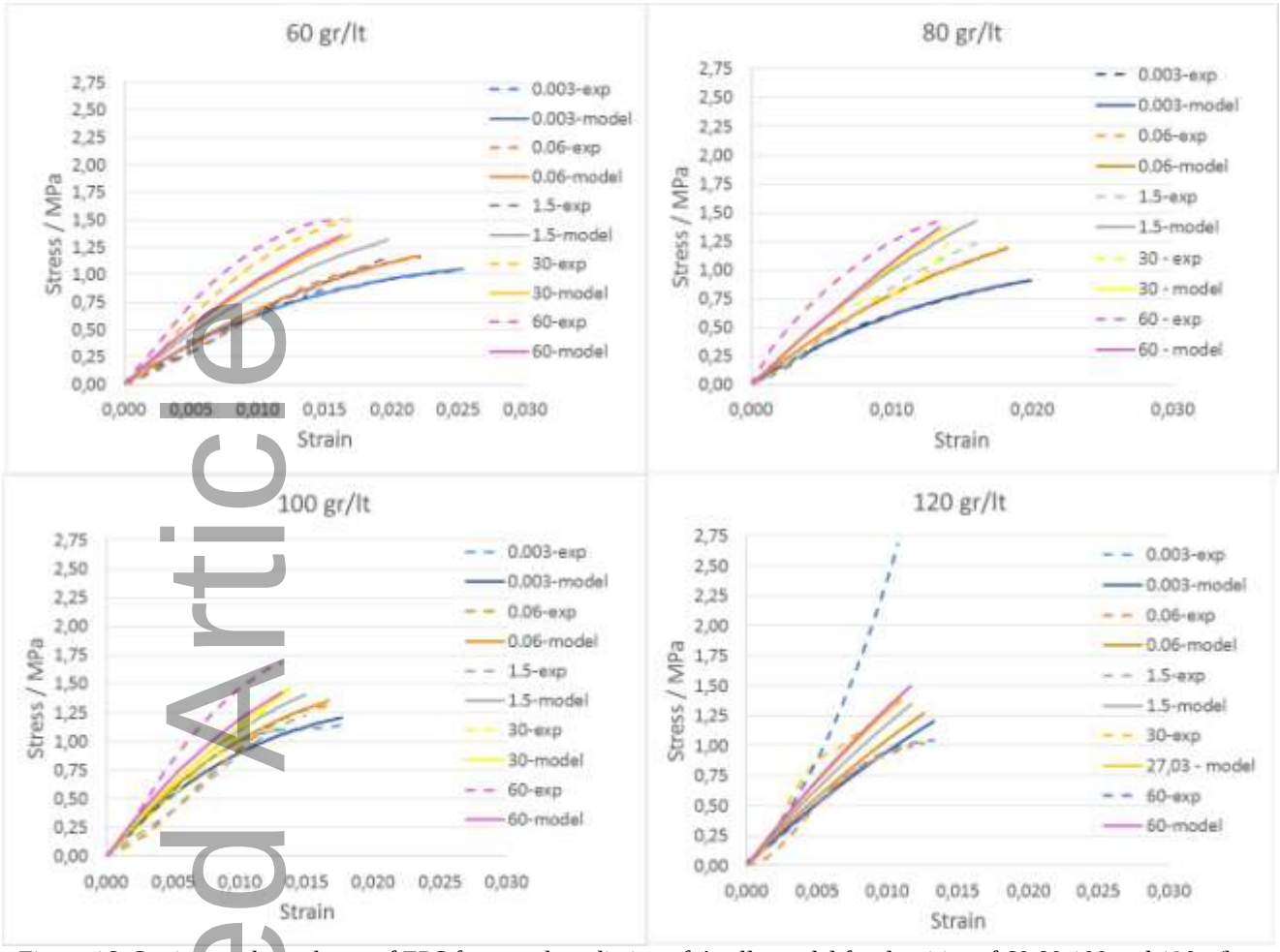

Figure 16: Strain rate dependency of EPS foam and prediction of Avalle model for densities of 60,80,100 and 120 g/l

A deviation is noticed for high strain rates. if the damping solution is not used for all densities. The force oscillations are therefore still significant and they can influence the UTS. However as mentioned earlier the presence of a damper reduces the oscillations and as a result the UTS allowing better fit between experimental and theoretical results as predicted by the Avalle model. At the density of 80 and 100 g/l, damped curves for the strain rate 60 s^{-1} have been tested. The parameters E, A and m have been estimated again using the same method. If we compare the model prediction to the experimental dampened curves, the model does indeed match the experimental curves at the highest strain rates. The quality of fit for the different strain rates and densities is shown in Tables 8-11 where the Root Mean Square Error (RMSE) and the normalized RMSE (N-RMSE) values are calculated according to the functions:

$$RMSE = \sqrt{\frac{\sum_{i=1}^{n}(y_i - Y_i)^2}{n}} \qquad \textit{(Equation 11)}$$

$$NRMSE = \frac{RMSE}{y_{max} - y_{min}} \qquad \textit{(Equation 12)}$$

where y is the predicted value, Y is the observed value of the model and n is the number of measurements.

Table 8: Calculated RMSE and N-RMSE values for density of 60 g/l

Strain rate (s^{-1})	RMSE	N-RMSE	Quality of fit
0.03	0,0215	0,0206	97,94%
0.07	0,0748	0,0646	93,51%
1.5	0,1550	0,1347	86,53%
30	0,1851	0,1466	85,34%
30 (Filtered)	0,1589	0,1348	86,52%
60	0,3819	0,2016	79,84%
60 (Filtered)	0,2799	0,1601	83,99%

Table 9: Calculated RMSE and N-RMSE values for density of 80 g/l

Strain rate (s^{-1})	RMSE	N-RMSE	Quality of fit
0.03	0,0331	0,0355	96,45%
0.07	0,0529	0,0452	95,48%
1.5	0,1504	0,1362	86,38%
30	0,2178	0,2151	78,49%
30 (Damped)	0,1389	0,1378	86,22%
30 (Filtered)	0,1233	0,1002	89,98%
60	0,1372	0,0869	77,39%
60 (Damped)	0,1650	0,1567	84,33%
60 (Filtered)	0,3251	0,1626	83,74%

Table 10: Calculated RMSE and N-RMSE values for density of 100 g/l

Strain rate (s^{-1})	RMSE	N-RMSE	Quality of fit
0.03	0,0570	0,0497	95,03%
0.07	0,1060	0,0813	91,87%
1.5	0,1805	0,1474	85,26%
30	0,1235	0,0871	91,29%
30 (Damped)	0,0561	0,0383	96,17%
30 (Filtered)	0,1315	0,0784	92,16%
60	0,3373	0,1651	83,49%
60 (Damped)	0,2402	0,1348	86,52%
60 (Filtered)	0,1800	0,1103	88,97%

Table 11: Calculated RMSE and N-RMSE values for density of 120 g/l

Strain rate (s^{-1})	RMSE	N-RMSE	Quality of fit
0.03	0,0277	0,0265	97,35%
0.07	0,1127	0,1096	89,04%
1.5	0,1412	0,1382	86,18%
30	0,1939	0,1690	83,10%
30 (Filtered)	0,1015	0,0842	91,58%
60	0,6397	0,2718	57,21%
60 (Filtered)	0,3819	0,2198	69,63%

4. Conclusions

The tensile properties of EPS foam at various densities and a wide range of strain rates have been studied. The standard High-Speed test machine (Instron 8502) was not adequate to achieve high displacement rates,

therefore, an alternative method was developed for testing EPS testing at high strain rates (30 – 60 s^{-1}) and successfully validated. The method consists of a drop-weight system where a mass is dropped from a certain height and can accelerate to the desired speed. The mass hits and accelerates a mechanism (impact block) and transfers a tensile load to the specimen. The force oscillations detected by the load cell were eliminated by using a rubber damper between the two colliding masses. A Fourier transform analysis and a low pass filter also proved to effectively filter out the oscillations.

It is important to obtain accurate strain data in tensile tests on foams: the small displacements are sensitive to any error or tolerance in the set-up and hence the crosshead displacement should not be used. The use of strain mapping based on digital image correlation provides an accurate and contactless alternative, valid over a wide range of strain rates, provided the sampling rate of the cameras is high enough for the required field of view.

Tensile stress-strain data over a wide range of strain rates (0.03 to 60 s^{-1}) were obtained for EPS foams related to impact energy absorption applications (60-120 gr/l). Compared to the scarce data found in literature, it was verified that the compression/tensile strength and the Young's modulus of polymer foams increases with increasing strain rate and density [3][11][17][19]. An opposite relationship was observed for strain at failure [19][11]. The absorbed fracture energy observed to reduce only slightly with increasing strain rate providing the excellent suitability of EPS foam for impact loading. At low strain rates the UTS did not show the expected increase with increasing density. Even though the general trend is verified, the Elastic modulus was slightly decreased from density 100 gr/l to 120 gr/l for strain rate 60 s^{-1}.

Of all the models available in literature, the Avalle model is the most comprehensive, as it takes into account strain rate dependence and allows a description of tensile and compressive behavior. It is therefore best suited as material model for FEA

The experimental data from all samples were used to calculate the model's parameters for each density. The reference strain rate has an important influence on the values and the variance of the model parameters. Scatter found on the obtained parameter values, demonstrates the need for more extensive experimental data.

REFERENCES

[1] Avalle M., Belingardi G., Montanini R, International. Journal of Impact Engineering **2001,** *25,* 455.

[2] Di Landro L., Sala G., Olivieri D, Polymer Testing **2002**, *21*,217.

[3] Lorna A. Gibson J., Cambridge University Press, **1997,**2nd edition.

[4] Gnip Y. Vejelis S., Kersulis V., Vaitkus S. Polymer Testing, **2007**,*26*,886.

[5] Pellegrino A. Tagarielli V. L. Gerlach R. Petrinic N.,International Journal of Impact Engineering **2015,***75*,214

[6] Walter T.R, Richards W. A. Ghatu S., Journal of Engineering Materials and Technology **2009,***131*,1.

[7] Horvath J, Geotextiles and Geomembranes **1994,***13,* 263.

[8] Ouellet S, Cronin D, Worswick M., Polymer Testing **2006** *25*,731.

[9] Duškov M. Geotextiles and Geomembranes **1997,***15*,147

[10] Croop B, Lobo H. Proceedings of 7th European LS-DYNA conference, **2009**.

[11] Wensu C. Hong H. Hughes D. Shi Y. Cui J. Li Z. Materials and Design, **2015,** *69*,170

[12] ISO 1926: Rigid cellular plastics - Determination of tensile properties, Switzerland: ISO International Standard, **2009**.

[13] ASTM D638-14, Standard Test Method for Tensile Properties of Plastics, ASTM International, West Conshohocken, PA, **2014**

[14] Gong, F.Q. & Li, X.B. Chinese Journal of Rock Mechanics and Engineering **2010,** *29*,2076

[15] Forsström A. Bossuyt S. Scotti G. Hänninen H. Experimental Mechanics **2019,** *1*

[16] Koerber, H. Xavier, J. Mechanics of Materials **2010,***42*,1004

[17] Ling C. Ivens J. Cardiff P. Gilchrist M. , International Journal of Mechanical Sciences **2018,***144*,480

[18] Hensley S. , Mackenzie C. , Small S. Archer D. , Lakes E. , Rogge R., Acta of Bioengineering and Biomechanics **2017,***19*,187

[19] Castiglioni A. Castellani L.,Cuder G. Comba S. Colloids and Surfaces A: Physicochemical and Engineering Aspects, **2017,***534*,71

[20] Jeong Y. K. Cheon S. S. , Journal of Mechanical Science and Technology, **2012,***26*,2033

[21] Chen C. Lu T.J., Fleck N.A., Journal of the Mechanics of Physics of Solids, **1999,***47*,2235

[22] Choonghee J. Jin F. Hani E. Naguib., Poylmer **2005,***46*,11896

[23] Liu Q. Subhash G., Society of Plastics Engineers, Polymer Engineering & Science **2004,** *44*,463

[24] Avalle M., Belingardi G., Ibba A., International Journal of Impact Engineering **2007,***34*,3

[25] Nagy A., Ko W.L., Lindholm U.S. , Journal of Cellular Plastics **1974**,10,127

[26] McCormick N. , Materials today, **2010**,13,52

[27] Mills N.J. & Kang P. *Cellulal Plasics.* **1994** 30, 196–222.

[28] Koumlis S. Lamberson L. , Experimental Mechanics **2019**,1

[29] Jeon I, Yamadab Y, Yamadab T, Katou K, Sonoda T, Asashina T Experimental Analysis of Nano and Engineering Materials and Structures **2007**,773-774

[30] Youming C. Battley M. International Journal of Engineering Science **2017**,120,220-240

Table of Contents

Expanded polystyrene (EPS) foam is often used in a range of applications including crush. However, its tensile properties have not yet been studied thoroughly. In this study, static and dynamic tension tests are conducted on dog-bone samples for densities between 60-120 g/l and strain rates between 0.003-60 s^{-1}. The

influence of both parameters on Stress-Strain behavior, Dynamic Strength, Young's modulus and Energy Absorption is defined. The experimental results are compared with the predictions of a constitutive model for crushable foams. The quality of fit obtained between experimental and theoretical results is between 70% - 97% depending on the strain rate.

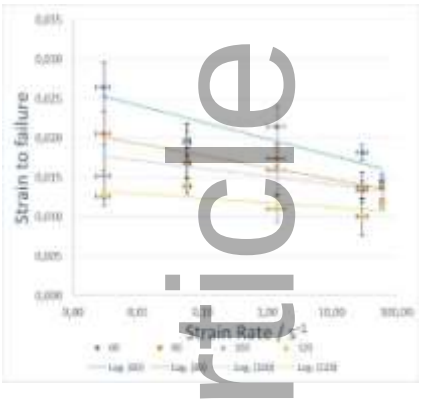

Keywords: polystyrene, tensile, properties, strain rate, density